

## ■ Dye-Sensitized Solar Cells

# A Computational and Experimental Study of Thieno[3,4-b]thiophene as a Proaromatic $\pi$ -Bridge in Dye-Sensitized Solar Cells

Phillip Brogdon,<sup>[a]</sup> Fabrizio Giordano,<sup>[b]</sup> George A. Punecky,<sup>[a]</sup> Amala Dass,<sup>[a]</sup> Shaik M. Zakeeruddin,<sup>[b]</sup> Mohammad Khaja Nazeeruddin,<sup>[b]</sup> Michael Grätzel,<sup>[b]</sup> Gregory S. Tschumper,<sup>[a]</sup> and Jared H. Delcamp<sup>\*[a]</sup>

**Abstract:** Four D- $\pi$ -A dyes (D=donor, A=acceptor) based on a 3,4-thienothiophene  $\pi$ -bridge were synthesized for use in dye-sensitized solar cells (DSCs). The proaromatic building block 3,4-thienothiophene is incorporated to stabilize dye excited-state oxidation potentials. This lowering of the excited-state energy levels allows for deeper absorption into the NIR region with relatively low molecular weight dyes. The influence of proaromatic functionality is probed through a computational analysis of optimized bond lengths and nucleus independent chemical shifts (NICS) for both the

ground- and excited- states. To avoid a necessary lowering of the TiO<sub>2</sub> semiconductor conduction band (CB) to promote efficient dye-TiO<sub>2</sub> electron injection, strong donor functionalities based on triaryl- and diarylamines are employed in the dye designs to raise both the ground- and excited-state oxidation potentials of the dyes. Solubility, aggregation, and TiO<sub>2</sub> surface protection are addressed by examining an ethyl-hexyl alkyl chain in comparison to a simple ethyl chain on the 3,4-thienothiophene bridge. Power conversion efficiencies of up to 7.8% are observed.

## Introduction

Since the introduction of dye-sensitized solar cells (DSCs) in 1991,<sup>[1]</sup> tremendous efforts have been made to bring DSCs to the forefront of alternative energy options.<sup>[2]</sup> The basic operating principle of a DSC device involves injection of electrons from a photoexcited dye molecule into a metal oxide semiconductor (typically TiO<sub>2</sub>). The electron then traverses an external circuit to a counter electrode, where it is transferred back to the dye molecule through the use of a redox shuttle, such as the I<sup>-</sup>/I<sub>3</sub><sup>-</sup> couple.<sup>[3]</sup> The dye plays many crucial roles, including controlling the light absorbed and charge separation, which directly affects power output.

Traditionally, ruthenium-based sensitizers have dominated the DSC dye-design field by providing the highest device power conversion efficiencies (PCEs of approximately 11%).<sup>[4–6]</sup> Recently, metal-free organic dyes **ADEKA-1**<sup>[7a]</sup> and **C275**<sup>[7b]</sup> and

a porphyrin-based dye **SM315**<sup>[8]</sup> have demonstrated record PCEs of 12.5–13.0% without the use of precious metals. The success of these dyes is largely driven by the iterative use of the ubiquitous, modular D- $\pi$ -A dye design (D=donor, A=acceptor). PCE improvements over these impressive devices is reasonable and would be aided through the careful development of building blocks to allow tunable access to the NIR region of the solar spectrum.<sup>[9]</sup> Proaromatic building blocks are promising dye components that allow for tunability into the NIR region from relatively low molecular weight dyes.

Several DSC photosensitizers have recently employed the use of proaromatic structures.<sup>[8,11–13]</sup> These structures benefit from added stability provided by a region of local aromaticity in their excited-state (Figure 1). Due to this aromatically stabilized excited state, photoexcitation occurs at significantly lower energies, which leads to a narrowed optical bandgap. The proaromatic conjugated building block 3,4-thienothiophene (3,4-TT) has been explored recently in several polymer applications as a low-band-gap material for organic photovoltaic devices,<sup>[14–16]</sup> and only once in DSC devices as a  $\pi$ -bridge with an encouraging PCE (3.7%).<sup>[12]</sup>

Proaromatic materials often absorb longer wavelengths of light than aromatic materials of similar conjugation length. This attractive attribute is accomplished through the stabilization of excited-state oxidation potentials ( $E_{(S^+ / S^*)}$ , Table 1). However, a balance is needed between stabilizing  $E_{(S^+ / S^*)}$  values to absorb shorter wavelengths and maintaining a necessary overpotential ( $\Delta G_{inj}$ ) for efficient electron injection from a dye excited state to the TiO<sub>2</sub> conduction band (CB). A prior study on

[a] P. Brogdon,<sup>†</sup> G. A. Punecky, Dr. A. Dass, Prof. G. S. Tschumper, Prof. J. H. Delcamp  
Department of Chemistry and Biochemistry  
University of Mississippi, University, MS 38677 (USA)  
E-mail: delcamp@olemiss.edu

[b] Dr. F. Giordano,<sup>†</sup> Dr. S. M. Zakeeruddin, Prof. M. K. Nazeeruddin, Prof. M. Grätzel  
Laboratory for Photonics and Interfaces  
Swiss Federal Institute of Technology, 1015 Lausanne (Switzerland)

[†] Authors contributed equally.

Supporting information for this article is available on the WWW under <http://dx.doi.org/10.1002/chem.201503187>.

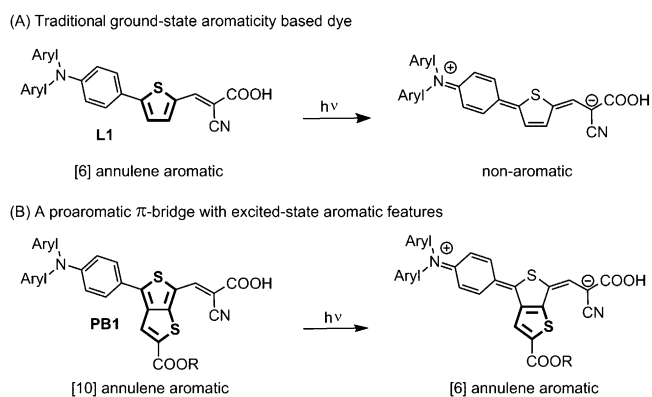


**Figure 1.** A comparison of a D- $\pi$ -A dye designed with common aromatic building blocks (such as **L1**<sup>[10]</sup>) with a dye containing a proaromatic building block (**PB1**) leading to competing aromatic ground and excited states.

**Table 1.** Optical and electrochemical data for **PB1**, **PB2**, **DP1** and **DP2**.

	Absorbance data <sup>[a]</sup>			Electrochemical data		
	$\lambda_{\text{max}}$ [nm]	$\epsilon$ [M <sup>-1</sup> cm <sup>-1</sup> ]	$\lambda_{\text{onset}}$ [nm] <sup>[b]</sup>	$E_{\text{S}+/S}$ [V] <sup>[c]</sup>	$E_{\text{S}+/S^*}$ [V] <sup>[d]</sup>	$E_{\text{g}}^{\text{opt}}$ [eV] <sup>[e]</sup>
<b>PB1</b>	560	26000	665	+1.09	-0.79	1.88
<b>PB2</b> *	584	30000	670	+1.08	-0.77	1.85
<b>DP1</b>	558	22000	650	+1.09	-0.79	1.88
<b>DP2</b>	591	20000	670	+1.08	-0.77	1.85
<b>MCT-1</b> <sup>[f]</sup>	524	23000	600	+1.35 <sup>[g]</sup>	-0.70	2.05
<b>FTT-1</b> <sup>[f]</sup>	509	35000	590	+1.41 <sup>[g]</sup>	-0.71	2.12
<b>LS-1</b> <sup>[h]*</sup>	483	20000	610	+0.96	-1.21	2.17

[a] Measurements made in DCM. [b] The absorption onset ( $\lambda_{\text{onset}}$ ) was taken at the intercept of a tangent line on the low energy side of the  $\lambda_{\text{max}}$  absorption curve and the baseline. [c]  $E_{\text{S}+/S}$  measurements were made in DCM with a 0.1 M  $\text{Bu}_4\text{NPF}_6$  electrolyte and ferrocene as an internal standard. All values are reported versus NHE. [d]  $E_{\text{S}+/S^*}$  was calculated from the equation  $E_{\text{S}+/S^*} = E_{\text{S}+/S} - E_{\text{g}}^{\text{opt}}$ . [e]  $E_{\text{g}}^{\text{opt}}$  was calculated from the equation  $E_{\text{g}}^{\text{opt}} = 1240/\lambda_{\text{onset}}$ . [f] **MCT-1** measurements are taken from reference [12]. Optical data and electrochemical data are reported in THF. [g] Ground-state oxidation potentials calculated from the  $E_{0-0}$  and  $E_{0-0}^*$  values reported in reference 12. [h] **LS1** measurements are reported in reference [17] below. **LS1** has an identical structure to **DP2** and **PB2** with the 3,4-TT proaromatic bridge substituted with a simple thiophene. Note: reference [17] uses a ferrocene reference set to +0.4 V vs. NHE. For consistency in this manuscript, we have calibrated the **LS1** numbers in our table to a ferrocene reference of +0.7 V vs. NHE as reported by Gieger and co-workers<sup>[18]</sup> with a conversion of SCE to NHE by addition of +0.24 V. \*Denotes that the dyes are identical with the exception of changing the proaromatic 3,4-TT bridge to a thiophene.

3,4-TT showed low energy  $E_{\text{S}+/S^*}$  values that require the addition of excessive  $\text{Li}^+$  to lower the  $\text{TiO}_2$  CB to boost  $\Delta G_{\text{inj}}$  values. This results in low device open-circuit voltage values and diminished PCEs. Coarse tuning of  $E_{\text{S}+/S^*}$  values may be accomplished through the selection of electron-deficient functionalities; however,  $E_{\text{S}+/S^*}$  values may be finely tuned through donor building block selection. Increasing electron-donating strength often leads to a weak destabilization of the dye  $E_{\text{S}+/S^*}$  values. A series of four dyes based on 3,4-TT with strong donor motifs dihexyloxytriphenylamine (TPA) and indoline were selected as target materials. The concise indoline donor was selected to compare with the larger triphenylamine donor

in order to evaluate if PCE diminishing aggregative effects were present in final devices. Additionally, the alkyl groups on the 3,4-TT ester  $\pi$ -bridge were varied in combination with each donor to evaluate the structure–performance relationship of longer versus shorter chain length on DSC device PCE.

## Results and Discussion

The synthesis of the **PB** (ethylhexyl-substituted 3,4-TT) and **DP** (ethyl-substituted 3,4-TT) series (depicted in Figure 2) proceeds

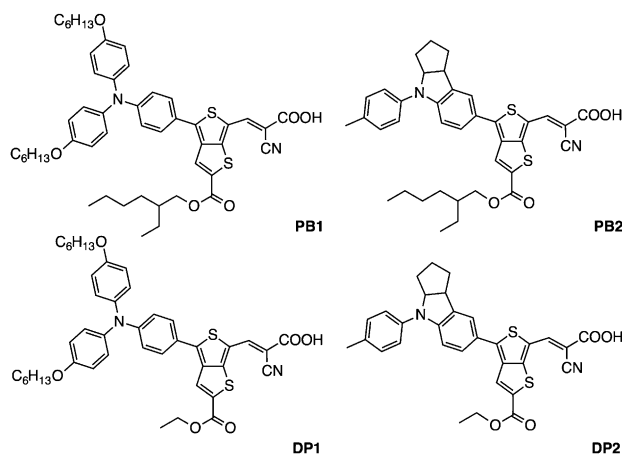
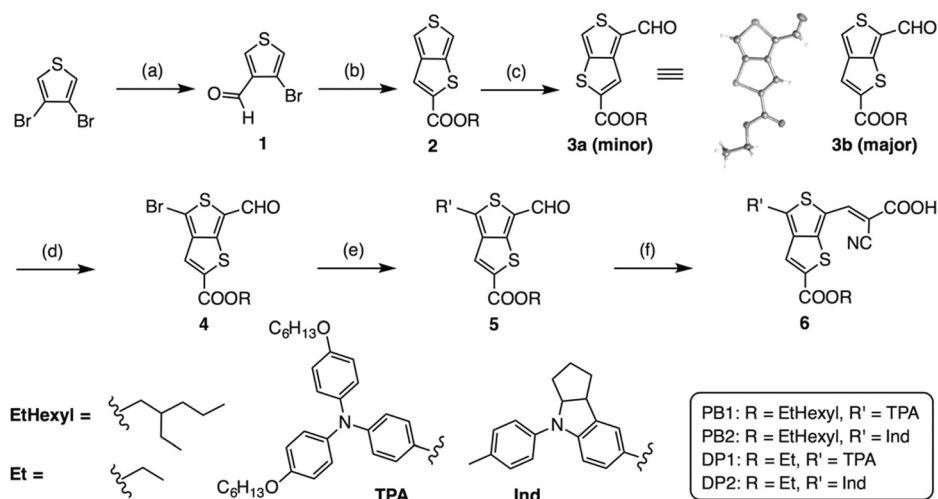


**Figure 2.** Target dye structures with varying donor groups and chain lengths on the proaromatic 3,4-TT  $\pi$ -bridge with cyanoacrylic acid.

in six synthetic steps according to Scheme 1. Lithium halogen exchange with commercially available 3,4-dibromothiophene and quenching with DMF leads to bromoaldehyde **1**. A one-pot Cu-catalyzed thiol cross-coupling/condensation reaction to close the ring forms the 3,4-TT ester **2**. The subsequent Vilsmeier–Haack reaction on **2** yields two regioisomers **3a** and **3b** (in a 1:2 mixture), which vary by orientation of the proaromatic ring sulfur on the opposite (**3a**) or same side (**3b**) as the aldehyde. The <sup>1</sup>H NMR of these isomers yields three singlets in the aromatic region with only slight shifts in ppm values for each isomer. To unambiguously assign the structure to these isomers NOE NMR and X-ray crystallography techniques were employed. A slight NOE response is observed between the aldehyde-H and proaromatic thiophene-H for isomer **3a** with no NOE response observed for any of the hydrogens in **3b** (Figure 3). X-ray quality crystals were obtained from isomer **3a** in toluene to give long yellow needles. The NOE NMR results and X-ray crystallography results both confirm the major isomer as desired product **3b** (Scheme 1). Aldehydes **3a** and **3b** are separable by silica gel chromatography with **3b** having a slightly lower  $R_f$ . This regioselective route proved reliably scalable to multiple gram batches of isomer **3b**.

Compound **3b** undergoes NBS bromination in good yield to give the bromoaldehyde **4** in four steps and 18% overall yield. Arylamine donor building blocks were installed through Suzuki coupling reactions in excellent yields to give intermediate **5**,



**Scheme 1.** Synthetic scheme for dyes **PB1**, **PB2**, **DP1**, and **DP2**. a) i. *n*BuLi (1.5 equiv), 0.25 M Et<sub>2</sub>O, -78 °C, 30 min; ii. DMF (excess), -78 °C to RT, 2 h; 74%. b) Ethylhexyl mercaptoacetate (or ethyl mercaptoacetate, 1.1 equiv), CuO nanopowder (3%), K<sub>2</sub>CO<sub>3</sub> (1.5 equiv), 0.5 M DMSO, 60 °C, 16 h; 56% (EtHexyl); 80% (Et). c) i. POCl<sub>3</sub> (1.05 equiv), DMF (1.05 equiv), 0.4 M DCE, 0 °C, 2.5 h; ii. 0.4 M KOH (1.0 M, aq), RT, 15 min; 48% (EtHexyl); 71% (Et). d) NBS (1.2 equiv), 0.2 M DMF, 0 °C to RT; 62% (EtHexyl); 82% (Et). e) TPA-Bpin (or Ind-Bpin, 1.1 equiv), K<sub>3</sub>PO<sub>4</sub> (3.0 equiv), [Pd<sub>2</sub>(dba)<sub>3</sub>] (4%), X-Phos (16%), 0.05 M toluene, 1.15 M H<sub>2</sub>O, 80 °C, 6 h; 75% (TPA-EtHexyl); 93% (TPA-Et); 84% (Ind-EtHexyl); 26% (Ind-Et). f) Cyanoacetic acid (3.0 equiv), piperidine (7.0 equiv), 0.06 M CHCl<sub>3</sub>, 90 °C; 77% (TPA-EtHexyl); 51% (TPA-Et); 63% (Ind-EtHexyl); 35% (Ind-Et).

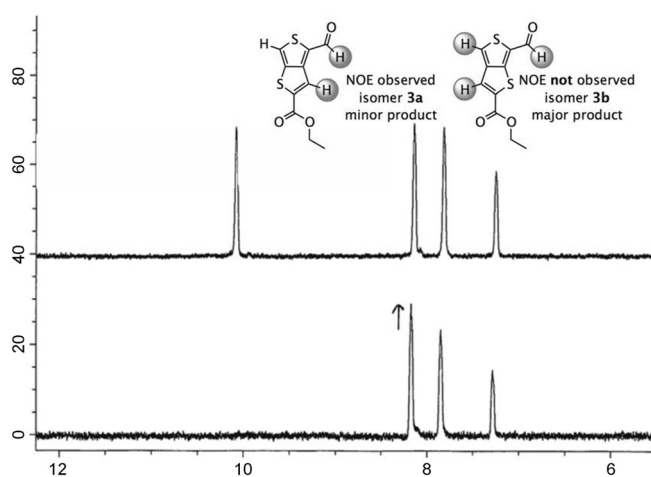


**Figure 3.** NOE NMR spectrum of intermediate **3a** (top) with the aldehyde proton irradiated (bottom).

and the final dyes (**PB1**, **PB2**, **DP1**, and **DP2**) were completed through Knoevenagel condensation with cyanoacetic acid (CAA) in high yield in six linear steps from commercial starting materials in up to about 13% overall yield.

### Optical and electrochemical data

UV/Vis absorption spectra were collected for **PB1**, **PB2**, **DP1**, and **DP2** in dichloromethane (Figure 4, Table 1). The use of dihexyloxyTPA as a strong donor on dye **DP1** gave a  $\lambda_{\max}$  and  $\lambda_{\text{onset}}$  of about 560 and 650 nm respectively. A longer alkyl chain with a stereogenic center on the 3,4-TT bridge (**PB1**) yielded identical  $\lambda_{\max}$  and  $\lambda_{\text{onset}}$  values to **DP1**; however, the molar absorptivity increased from 22 000 to 26 000 M<sup>-1</sup> cm<sup>-1</sup>.

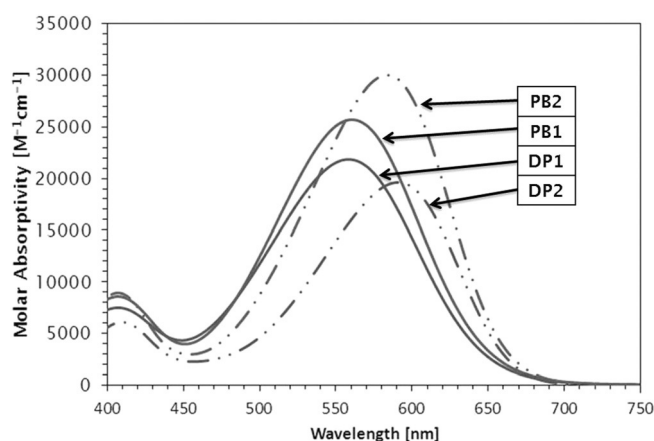


**Figure 4.** UV/Vis absorption spectra of **PB1**, **PB2**, **DP1** and **DP2** in dichloromethane.

This trend of increasing molar absorptivity is expected based on previous studies regarding an increase in alkyl chain length.<sup>[19]</sup> Installation of a stronger indoline donor in place of the dihexyloxyTPA donor of **DP1** and **PB1** resulted in red-shifted  $\lambda_{\max}$  and  $\lambda_{\text{onset}}$  values (by approximately 25 nm) for both **DP2** and **PB2**. Introduction of extended alkyl chains on the 3,4-TT bridge again resulted in higher molar absorptivity values for **PB2** than **DP2** with shorter alkyl chains (30 000 versus 20 000 M<sup>-1</sup> cm<sup>-1</sup>). Importantly, the dihexyloxyTPA and indoline donors show substantially diminished optical band gaps ( $E_g^{\text{opt}}$ ) when compared with a simple TPA donor on the 3,4-TT-CAA  $\pi$ -bridge-acceptor (about 1.85 versus 2.12 eV, Table 1). Dye **LS-1** (identical to **DP2** and **PB2** when the 3,4-TT  $\pi$ -bridge is replaced with a simple thiophene) was used for comparison of the proaromatic 3,4-TT with a common  $\pi$ -bridge (Table 1). A  $\lambda_{\max}$  red-shift of > 100 nm is observed when the 3,4-TT building

block is used, while the molar absorptivities are similar. Electrochemical analysis is conducted to better understand the effects of the 3,4-TT building block on the ground- and excited-state oxidation potentials when compared to thiophene.

Solvatochromic effects of the proaromatic 3,4-TT bridge were examined and compared to that of thiophene through the comparison of **PB2** and **LS1**, which differ only at the  $\pi$ -bridge (Figures 5 and 6 in the text and Tables S2 and S3 in the

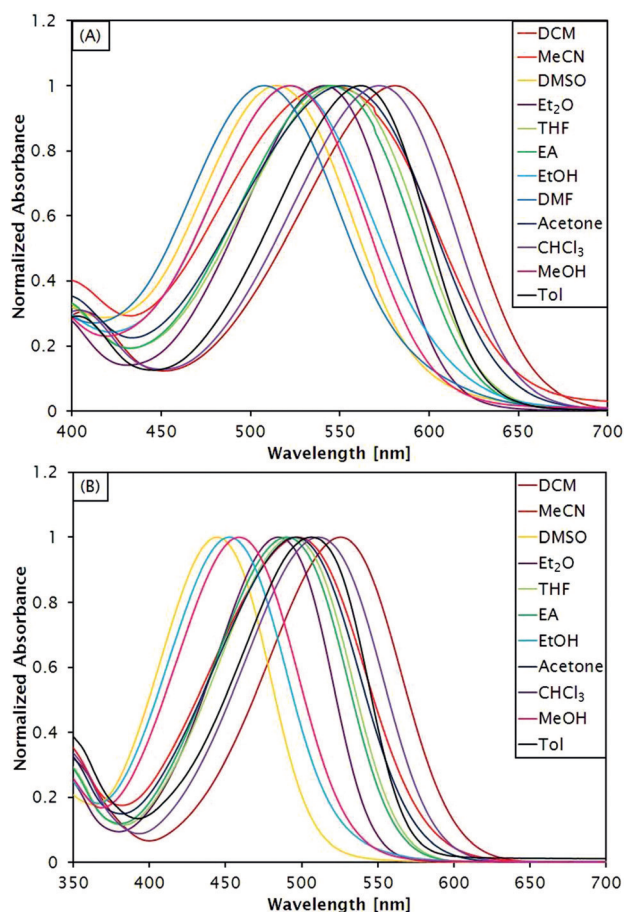


**Figure 5.** UV/Vis absorption spectra of **PB2** (A) and **LS1** (B) in various solvents. EA = ethyl acetate and Tol = toluene. The **LS1** absorption spectrum in DMF is omitted due to solubility issues, see Supporting Information for the spectrum.

Supporting Information). For both **PB2** and **LS1** the absorption maxima varied by approximately 100 nm with dichloromethane giving the longest wavelength absorption for both dyes and DMSO/DMF giving the shortest wavelength absorptions (Figure 5). This indicates that the solvent stabilization extent is similar between the two dyes in the ground-state geometry. It should be noted that a clear trend based on solvent polarity was not apparent. A substantial difference was noted when comparing the range of the emission maxima shifts in various solvents (Figure 6). The non-proaromatic **LS1** gave emissions over roughly a 125 nm range (approximately 0.24 eV), while **PB2** shows a relatively narrow emission range based on solvent of about 50 nm (approximately 0.11 eV) after excluding

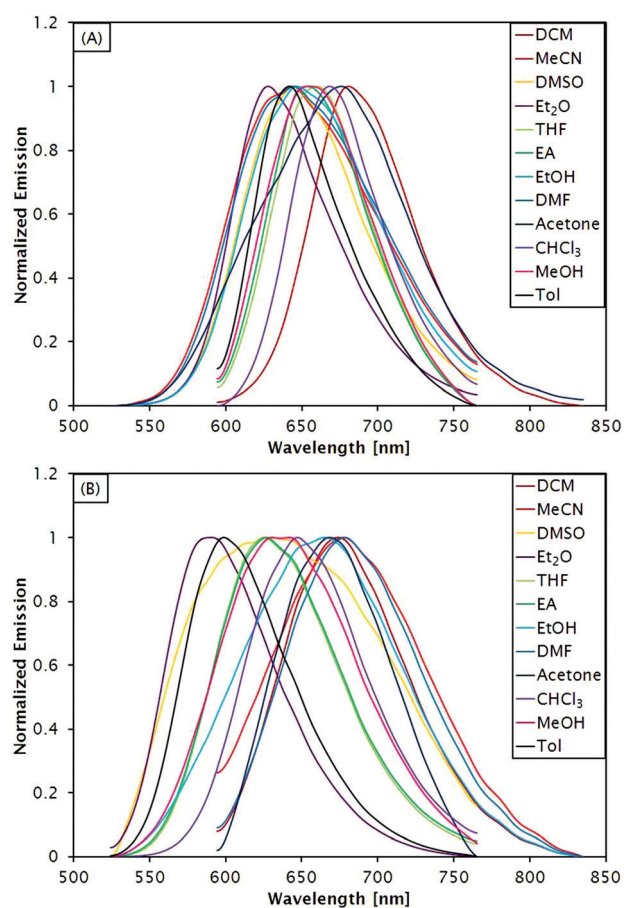


**Figure 6.** Emission spectra of **PB2** (A) and **LS1** (B) in various solvents. EA is ethyl acetate and Tol is toluene. The **LS1** absorption spectrum in DMF is omitted due to solubility issues, see Supporting Information for the spectrum.

the Et<sub>2</sub>O data point due to apparently low solubility. The difference in the solvatochromic effects of these two dyes were further highlighted through analysis of the Stokes shifts observed. Dye **LS1** gave Stokes shifts ranging broadly from 0.38 to 0.98 eV, while those of **PB2** were observed over a significantly narrower range of 0.27 to 0.52 eV. The dramatic difference in solvatochromic effects from the emission curve sets and Stokes shifts for these two dyes may in part be due to a weaker stabilization of the charge-separated excited-state from the solvent with proaromatic bridges as the dye excited-state is already stabilized by aromaticity.

The ground-state oxidation potentials ( $E_{(S+/S)}$ ) were measured to determine if suitable electron regeneration could take place between the dye and the  $I^-/I_3^-$  redox shuttle.  $E_{(S+/S)}$  values are critical in determining the thermodynamic driving force for dye regeneration ( $\Delta G_{reg}$ ) in a functioning DSC device and calculating  $E_{(S+/S^*)}$  values. Cyclic voltammetry was used to evaluate the ground-state oxidation potential of **PB1**, **PB2**, **DP1**, and **DP2** in DCM with a 0.1 M Bu<sub>4</sub>NPF<sub>6</sub> electrolyte (Table 1). Ground-state potentials were found to range from +1.08 to +1.09 V versus NHE. These potentials are substantially higher in energy than previously measured for unsubstituted TPA-3,4-TT dyes (+1.41 to +1.35 V vs. NHE).<sup>[12]</sup> Thus, a lower

overpotential for  $\Delta G_{\text{reg}}$  of 0.73–0.74 eV is observed for the **PB** and **DP** dyes. The optical band gap for these dyes ranged from 1.88–1.85 eV with **PB2** and **DP2** having the narrowest bandgap. The excited-state potentials (–0.77 to –0.79 V vs. NHE) are calculated from the equation  $E_{(S_1/S_0)} = E_{(S_0/S_0)} - E_g^{\text{opt}}$  and show a desirable electron injection driving force into the  $\text{TiO}_2$  conduction band ( $\Delta G_{\text{inj}} = 0.27\text{--}0.29$  eV, Figure 7). It is worth noting that the

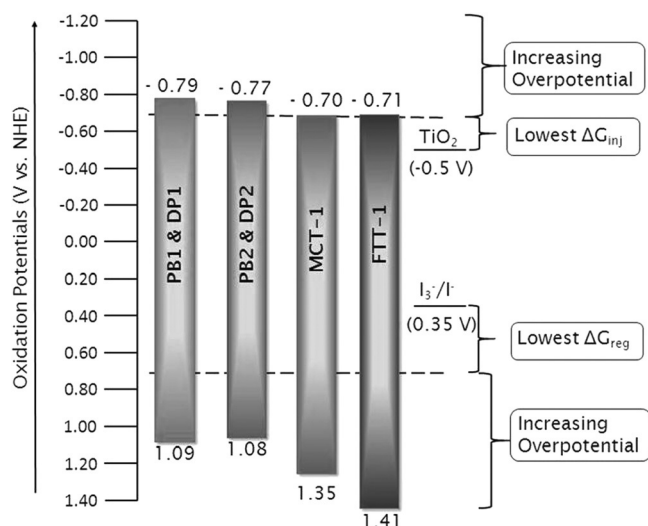


**Figure 7.** Comparison of ground-state (positive values) and excited-state (negative values) oxidation potentials of **PB** and **DP** series dyes with previously reported **MCT-1** and **FTT-1**. Values for **MCT-1** and **FTT-1** are reported as shown in Table 1 of Reference [12] with the ground-state oxidation potentials calculated from the  $E_{0-0}$  and  $E_{0-0}^*$  reported therein.

$E_{(S_1/S_0)}$  values are similar for the 3,4-TT dyes **PB2/DP2** and the non-pro-aromatic dye **LS-1** (within  $\approx 100$  mV); however, the  $E_{(S_1/S_0)}$  values are dramatically shifted by  $>400$  mV to more stable values energies when the proaromatic 3,4-TT bridge is incorporated into the dye structure.

### Computational studies

In addition to well-positioned oxidation potentials, dyes should also have an orbital distribution that allows for electron injection into  $\text{TiO}_2$  and restrict back electron transfer. Ideally, the LUMO should be positioned near the acceptor/anchor at the  $\text{TiO}_2$  surface to allow for efficient injection and the HOMO should be centered predominately on the donor and spatially separated from the  $\text{TiO}_2$  surface to diminish back electron transfer from the  $\text{TiO}_2$  semiconductor.<sup>[2]</sup> DFT calculations employing the B3LYP functional and 6-311G+(d,p) basis set show an orbital arrangement that is ideal for electron injection into the  $\text{TiO}_2$  semiconductor. As shown in Figure 8, the HOMO is centered on the donor region and the LUMO is centered on the acceptor side of the dye for both **PB1/DP1** and **PB2/DP2** analogues as well as for the fully alkylated **PB1**, **FTT-1** and **L1** (see Supporting Information). The HOMO and LUMO orbitals appear to have good overlap across the 3,4-TT bridge as a significant accumulation of orbital density is present for both the

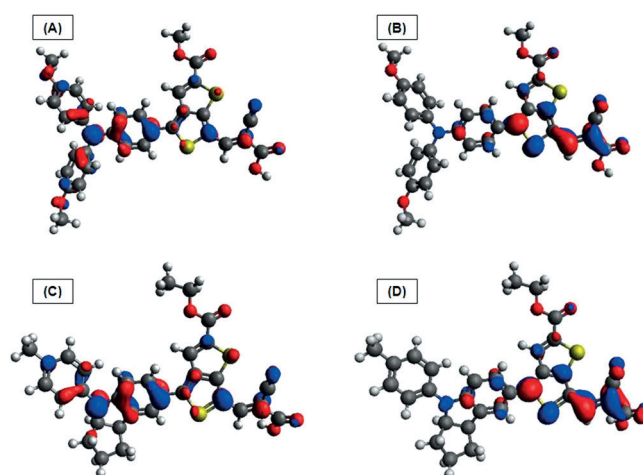


**Figure 8.** HOMO (A) and LUMO (B) of **PB1/DP1** analogues as well as HOMO (C) and LUMO (D) of **PB2/DP2** analogues. All extended alkyl chains were truncated to methyl chains. Iso values set to 0.04. See Supporting Information for orbitals of **L1**, **FTT-1** and fully alkylated **PB1**.

HOMO and LUMO, which suggests efficient intramolecular charge transfer is feasible. In order to examine the validity of the valence bond theory argument in Figure 1 for proaromatic materials exhibiting excited-state aromaticity, DFT and TD-DFT computations with the B3LYP/6-311+G(d,p) functional/basis set were performed to probe the aromaticity in the singlet ground state ( $S_0$ ) as well as the first excited singlet ( $S_1$ ) and triplet ( $T_1$ ) states of the 3,4-TT CT dyes and in comparison with **L1**. For example, valence bond theory suggests bonds 4 and 5 (Figure 9) will elongate upon excitation to the  $S_1$  state as

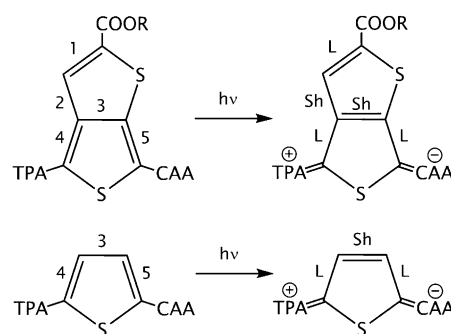


**Figure 9.** Comparison of 3,4-TT bond lengths in **PB1/DP1** and **L1** dyes in ground state versus the singlet excited state. TPA is bis(methoxyphenyl)phenylamine and CAA is cyanoacrylic acid. Sh = shortens; L = lengthens.

double-bond character is lost due to intramolecular charge transfer (ICT). Conversely, bond 3 is expected to shorten as the donor/acceptor-substituted thiophene loses local aromaticity. These predicted bond-length changes are indeed observed when the DFT optimized  $S_0$  structure of **PB1** is compared to the corresponding TD-DFT optimized  $S_1$  and  $T_1$  structures. Similar changes for **L1** are predicted and observed with an overall decrease in analogous bond-length change (Table 2). The full set of computed bridge-related bond-length changes for both

Bond	$S_0$ [Å]	$S_1$ [Å]	$\Delta R_{S_1}$ [Å]	$T_1$ [Å]	$\Delta R_{T_1}$ [Å]
dye: <b>PB1/DP1</b> analogue					
1	1.361	1.373	0.012	1.379	0.018
2	1.430	1.425	-0.006	1.416	-0.014
3	1.433	1.426	-0.007	1.408	-0.024
4	1.399	1.416	0.018	1.442	0.043
5	1.397	1.411	0.014	1.437	0.040
dye: <b>L1</b>					
3	1.401	1.394	-0.006	1.369	-0.032
4	1.390	1.391	0.001	1.419	0.029
5	1.391	1.408	0.017	1.443	0.052

dyes are shown in Table 2. The C–C bond lengths of the proaromatic thiophene are shifted toward more homogeneous values, with the length of bond 1 increasing by 0.012 Å, while the lengths of bonds 2 and 3 decrease by 0.006 and 0.007 Å, respectively, for the  $S_1$  state. In further support of this analysis, C–C bonds 4 and 5 found in the donor–acceptor thiophene lengthen by 0.018 and 0.014 Å, respectively, upon losing aromaticity. The  $T_1$  state shows bond-length changes consistent with those for the  $S_1$  state, but slightly larger in magnitude.

Additionally, nucleus independent chemical shifts (NICS) have been computed as another means to assess changes in the aromaticity of these systems. Since first proposed in 1996,<sup>[20]</sup> a variety of NICS indices have been introduced as a means to quantify aromaticity based on magnetic criteria.<sup>[21]</sup> For (quasi-) planar organic ring systems, the  $zz$  component of the magnetic shielding tensor and the total isotropic absolute shielding evaluated at various points  $R$  Å above/below the geometric center of the ring (typically denoted  $\text{NICS}(R)_{zz}$  and  $\text{NICS}(R)$ , respectively) have emerged as effective metrics of aromaticity that can readily be computed with DFT methods in a variety of popular software packages.<sup>[21c,22]</sup> Unfortunately, TD-DFT magnetic shielding tensors are not as widely available, which prevents us from directly assessing the aromaticity in the  $S_1$  excited state of these 3,4-TT-based molecules. It is possible, however, to compute these  $\text{NICS}(R)$  and  $\text{NICS}(R)_{zz}$  values for the  $T_1$  excited state, because, unlike  $S_1$ , the different spin symmetry prevents variational collapse to the  $S_0$  ground state. Baird's Rule predicts that Hückel's  $\pi$ -electron-counting rules are reversed in both the  $S_1$  and  $T_1$  states when compared with the  $S_0$  state (i.e.,  $[4n]$  is aromatic and  $[4n+2]$  is antiaromatic in excited-states).<sup>[23]</sup> This expectation has, in fact, been verified computationally for benzene.<sup>[24]</sup> For vertical excitations (i.e., when the geometry of the excited states is constrained to that of the ground state), both the  $S_1$  and  $T_1$  states demonstrate strong antiaromatic character. Due to these similarities, analysis of the  $T_1$  state in this manner provides a correlated indicator of aromatic behavior in the  $S_1$  state, which is typically the most populated state in these types of dyes. Because of the difficulties in directly computing the NICS indices in the  $S_1$  excited state, the general strategy was adopted here to compare the  $S_0$  and  $T_1$  aromaticity of both 3,4-TT rings in **PB1/DP1**.

The B3LYP/6-311 + G(d,p) ground-state optimized geometry of the **PB1/DP1** and **PB2/DP2** with truncated alkyl chain analogues were used for all geometry and NICS computations. Evaluation of **PB1** with full alkyl chain lengths gave near identical NICS values when compared with the truncated alkyl chains of the **PB1/DP1** analogue indicating a minimal effect on proaromaticity in this system (see the Supporting Information for DFT geometries, TD-DFT evaluation, and NICS graphs). For comparison, **FTT-1** and **L1** dyes were analyzed with the same method/functional/basis set combination. The magnetic shielding tensor was computed at the geometric center of each ring as well as 20 evenly spaced points (0.25 Å apart) "above" and "below" the ring plane (41 points altogether) for both the  $S_0$  and  $T_1$  states with the same functional and basis set. These  $\text{NICS}(R)$  and  $\text{NICS}(R)_{zz}$  values are plotted in Figure 10 and in the

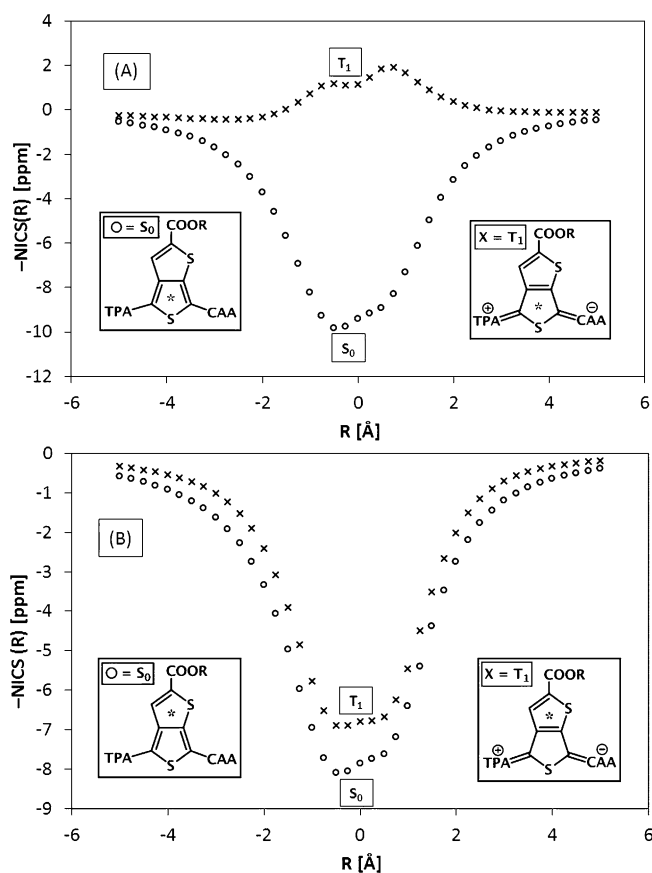


**Figure 10.** NICS( $R$ ) calculations demonstrating changes in aromaticity for 3,4-TT TPA/CAA-substituted thiophene ring (A) and the proaromatic thiophene ring (B) upon excitation to the  $T_1$  state. \* Denotes the ring undergoing NICS computational analysis at multiple points extending 5 Å above and below the plane of the ring.

Supporting Information, respectively, over the range spanning 5 Å "below" to 5 Å "above" the rings. The large negative isotropic NICS indices (ca. -9 ppm) at the center of the ring (i.e.,  $\text{NICS}(0)$ ), as well as slightly above and below the ring (e.g.,  $\text{NICS}(\pm 1)$ ) indicate both the TPA/CAA-functionalized thiophene ring and the proaromatic thiophene ring of 3,4-TT have appreciable aromatic character in the  $S_0$  state (○ data in Figure 10).

This is expected as the 3,4-TT building block has a 10- $\pi$  electron periphery (Figure 1). Upon vertical excitation to the  $T_1$  excited state, the TPA/CAA-functionalized thiophene ring experiences a significant decrease in aromaticity as the NICS( $R$ ) values near the ring plane become small in magnitude and even change sign ( $\times$  data in Figure 10a). Again, this is consistent with predictions from valence bond theory as charge is transferred from the donor to the acceptor, the local cyclic conjugation is lost. Interestingly, vertical excitation to the  $T_1$  state does not significantly change the aromatic character of the proaromatic ring of 3,4-TT as indicated by the similarity of the  $T_1$  ( $\times$ ) and  $S_0$  ( $\circ$ ) NICS( $R$ ) data in the bottom panel of Figure 10, signifying a preservation of aromaticity in the excited-state dye. This preservation of aromaticity leads to a stabilized excited-state energy and promotes longer wavelength absorption in these dyes when compared with dyes of similar conjugation lengths. Additional NICS computational analysis is available for **PB2/DP2**, **L1**, and **FTT-1** in the Supporting Information. Changes in NICS values based on the donor strengths of the aryl amine donors were subtle by NICS analysis.

TD-DFT was used to evaluate the influence of increasing donor strength in combination with a proaromatic  $\pi$ -bridge on the lowest energy vertical transition position and the oscillator strength. While additional effects such as alkyl chain length affect experimental values for molar absorptivities, computational evaluation shows primarily the electronic effects of the conjugated system irrespective of alkyl chains. Thus computational analysis was used to explore the effects of various donors and proaromatic versus aromatic bridges. Electron-donor strength proceeds in the following order: **FTT-1** < **PB1/DP1** < **PB2/DP2**. The changes in vertical transition are predicted to be subtle (< 0.1 eV difference); however, the changes in oscillator strength are apparent and follow the predicted donor strength trend ranging from 0.8537 to 0.9330. When the oscillator strengths of **L1** and **PB1** (analogous with the change of 3,4-TT to thiophene) are compared, that of the proaromatic system are significantly higher at 0.8775 versus 0.7506. The increase in oscillator strength may in part be attributed to the influence of the proaromatic bridge promoting a strong charge transfer.

### Device data

Having demonstrated favorable thermodynamic properties and orbital positions for the use of the 3,4-TT dye series in DSC devices, we then evaluated their performance in devices with  $\text{TiO}_2$  and  $\text{I}^-/\text{I}_3^-$  through I-V curve, incident photon-to-current conversion efficiency (IPCE), and electron lifetime measurements. As shown in Figure 11, the highest photocurrent density of the 3,4-TT series of dyes was observed with **DP2** followed by **PB2**, **PB1**, and **DP1** with a range of 13.7 to 10.9  $\text{mA cm}^{-2}$ . The red-shifted absorption of indoline-donor-based **DP2** and **PB2** in part leads to the enhanced photocurrent generation (Tables 1 and 3 and Figures 4 and 11). Dye **DP2** reached the highest peak IPCE value of 81%. Dyes **PB1** and **DP1** demonstrate noticeably lower photocurrent breadths when the IPCE was analyzed, which led to lower short-circuit current ( $J_{sc}$ )

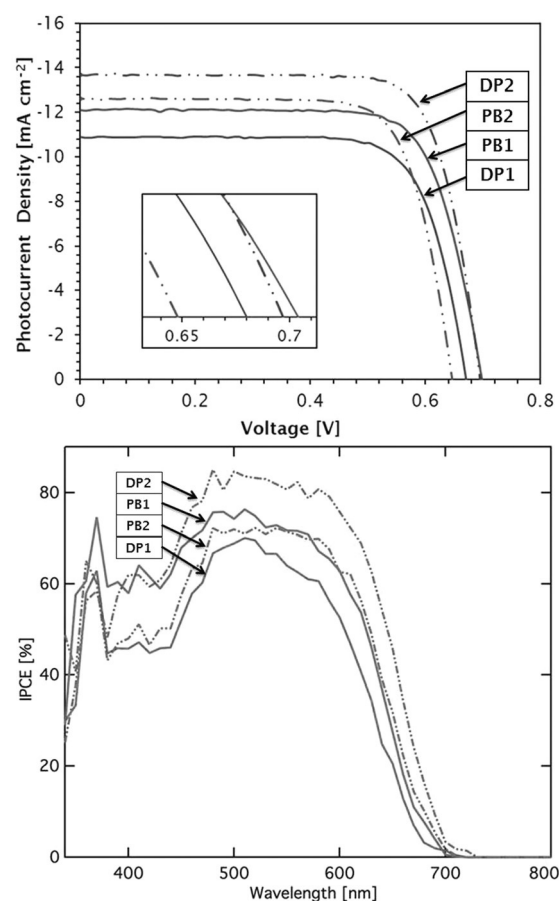


**Figure 11.** Top: J-V curve of dyes **PB1**, **PB2**, **DP1** and **DP2**. A 450 W Xe lamp at a simulated AM 1.5 G sun illumination was used as the light source. Electrolyte containing 1.0 M 1,3-dimethylimidazolium iodide (DMII), 100 mM LiI, 30 mM  $\text{I}_2$ , 0.5 M *tert*-butylpyridine, 0.1 M guanidinium thiocyanate (GNCS) in acetonitrile was used to measure **PB1**, **DP1**, **PB2** and **DP2**. Bottom: IPCE spectrum of **PB1**-, **PB2**-, **DP1**-, and **DP2**-based DSCs.

**Table 3.** Photovoltaic device<sup>[a]</sup> measurements under AM 1.5 G incident light.

	$V_{oc}$ [mV]	$J_{sc}$ [ $\text{mA cm}^{-2}$ ]	$FF$	PCE [%] <sup>[b]</sup>
<b>PB1</b>	704	12.1	0.75	6.50
<b>PB2</b>	648	12.7	0.75	6.24
<b>DP1</b>	680	10.9	0.75	5.61
<b>DP2</b>	697	13.7	0.76	7.41

[a] Devices fabricated using electrolyte containing 1.0 M 1,3-dimethylimidazolium iodide (DMII), 100 mM LiI, 30 mM  $\text{I}_2$ , 0.5 M *tert*-butylpyridine, 0.1 M guanidinium thiocyanate (GNCS) in acetonitrile. [b] PCEs were calculated using the formula:  $\frac{V_{oc} J_{sc} FF}{I_0}$ . All devices were measured at 1 sun.

values (Table 3, Figure 11). Dye **DP1** gave the lowest  $J_{sc}$  value due to a narrowed range of absorbance and the lowest IPCE peak value of 72%. The integrated IPCE spectrum areas are in good agreement with the values measured by the current-voltage curve. A dip in absorbance is seen for all dyes presented from 400–500 nm with **PB1** showing significantly better absorbance in this range allowing for a boost in  $J_{sc}$  relative to **DP1** with a similar IPCE onset (Table 3, Figure 11). The trend in

open-circuit voltages ( $V_{oc}$ ) observed is **PB1** > **DP2** > **DP1** > **PB2** and ranged from 704 to 648 mV. To better understand this trend in open circuit voltages, we studied electron lifetime versus capacitance trends to evaluate the dye structure effect on electron recombination rates with the redox shuttle (Figure 12). The longer alkyl chains present on 3,4-TT with **PB1**

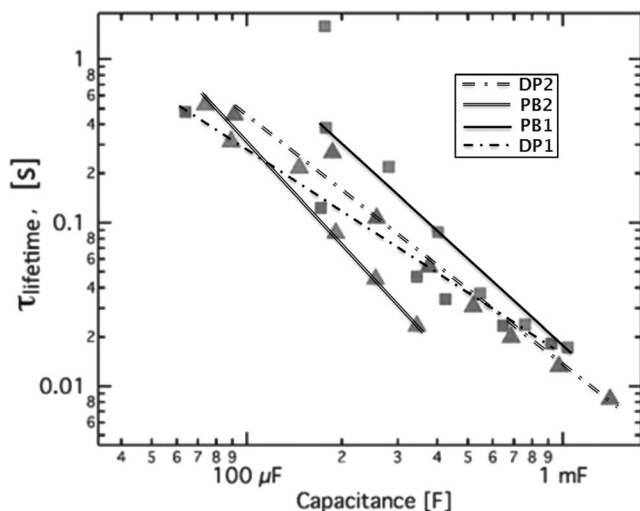


Figure 12. Electron lifetime versus capacitance of **PB1**, **PB2**, **DP1** and **DP2** based cells.

is shown to slow recombination between the redox shuttle and electrons present on the surface of  $TiO_2$  relative to **DP1**. The compact dye **DP2** with minimal alkyl chain lengths (one ethyl and one methyl) gave rise to a comparable electron lifetime to that of **DP1**. The shortest electron lifetimes were observed for **PB2**. Prior studies have shown introduction of a longer-alkyl-substituted group leads to longer electron lifetimes, which is attributed to slowing recombination of the redox shuttle with  $TiO_2$ .<sup>[25,26]</sup> Surprisingly, this is not observed with the ethylhexyl-substituted **PB2** as **DP2** demonstrates a longer electron lifetime with a simple ethyl group. This suggests PCE diminishing aggregative effects are not inhibitive for the 3,4-TT-bridge-based dyes as the more compact **DP2** gives improved electron lifetimes presumably through a closer packing of the dye on the  $TiO_2$  surface to allow for good surface protection from the redox shuttle. Dye **PB1** behaves as is typically expected, having the highest electron lifetime among all of the dyes measured due to the combined sterics of its ethylhexyl-substituted  $\pi$ -bridge and its hexyloxy-substituted TPA donor. This slow recombination rate allows **PB1** to generate a higher voltage relative to the other dyes in this series.

A  $V_{oc}$  increase of up to 144 mV and a  $J_{sc}$  increase of up to  $3.30 \text{ mA cm}^{-2}$  is observed for the **PB/DP** series when compared with previously reported 3,4-TT dyes. The success of the **PB/DP** series is owed to a destabilization of the excited-state potential and a narrowed optical band gap achieved through an increased donor strength (Figure 7). These potentials allow for more efficient injection of electrons into the  $TiO_2$  semiconductor CB as well as decreasing the dye regeneration excessive

overpotential from the  $I^-/I_3^-$  redox shuttle. Due to the increased energy of  $E_{(S^+/S^*)}$  for the **PB/DP** series,  $Li^+$  doping is not required to artificially lower the conduction band of  $TiO_2$  (100 mM LiI in **PB1/DP1** and **PB2/DP2**, 500 mM LiI in non-substituted triarylamine dyes). These improved electronic parameters lead to an overall increased performance ranging from 5.61% (**DP1**) to 7.41% (**DP2**) with a **DP2** champion cell reaching 7.8% PCE.

## Conclusion

We have synthesized four new dyes for use in DSC devices based on the 3,4-TT proaromatic building block. NOE NMR and X-ray crystallography studies were required to accurately characterize isomers resulting from a Vilsmeier–Haack reaction on the 3,4-TT building block. The valence bond theory prediction that an aromatic structure is present in the excited state of these proaromatic dyes was supported through computational analysis of bond lengths and NICS values in both the ground and excited states. The computational procedures set forward here will aid the development of future organic materials by allowing the evaluation of excited-state energy influences. Through judicious donor selection, we observed a decrease in the  $E_g^{opt}$  relative to analogous dyes with weaker donor strengths. We observe a noticeable red shift in the  $\lambda_{onset}$  of the more strongly donated indoline-based dyes (**PB2** and **DP2**) relative to their TPA-based counterparts (**PB1** and **DP1**). Higher  $V_{oc}$  values were obtained from DSC devices due to destabilization of the excited-state oxidation potentials allowing for efficient electron injection into the conduction band of  $TiO_2$  without the use of high  $Li^+$  concentrations. Through DFT calculations, it was determined that these dyes have ideal orbital arrangements for allowing electron injection into the  $TiO_2$  CB. These simple structural changes aided the 3,4-TT  $\pi$ -bridged dyes in reaching PCEs between 5.61–7.80%, which is a dramatic improvement for the 3,4-TT-based building block. In order to further improve PCEs of dyes containing 3,4-thienothiophene, work has begun on extending the conjugation length of these dyes through the implementation of simple  $\pi$ -bridges to extend absorption breadth. Furthermore, the use of cobalt redox shuttles allowing for higher maximum  $V_{oc}$  will be examined with the use of surface protecting donor groups.

## Experimental Section

**General information:** All commercially obtained reagents were used as received. 3,4-dibromothiophene was purchased from Matrix Scientific. Ethylhexyl mercaptoacetate was purchased from TCI. Thin-layer chromatography (TLC) was conducted with Sigma T-6145 pre-coated silica gel 60  $F_{254}$  polyester sheets and visualized with UV. Flash column chromatography was performed by Sorbent Tech P60, 40–63  $\mu\text{m}$  (230–400 mesh).  $^1\text{H}$  NMR spectra were recorded on a Bruker Avance-300 (300 MHz) spectrometer and a Bruker Avance-500 (500 MHz) spectrometer and are reported in ppm using solvent as an internal standard ( $\text{CDCl}_3$  at 7.26 ppm). Data reported as: s=singlet, d=doublet, t=triplet, q=quartet, p=pentet, m=multiplet, br=broad, ap=apparent, dd=doublet of doublets; coupling constant(s) in Hz; integration. UV/Vis spectra

were measured with a Cary 5000 UV/Vis spectrometer. Cyclic voltammetry was measured with a C-H Instruments electrochemical analyzer.

**Computational details:** All density functional theory (DFT) and time-dependent DFT (TD-DFT) data reported here were obtained with the B3LYP<sup>[27,28]</sup> exchange–correlation functional and the 6–311+G(d,p) basis set as implemented in Gaussian 09.<sup>[29]</sup> The B3LYP/6–311+G(d,p) magnetic shielding tensors were computed with the gauge-independent atomic orbital (GIAO) method.<sup>[30,31]</sup> Initial geometries for the **PB1**, **PB2**, **DP1** and **DP2** structures were obtained from MM2 optimizations in ChemBio3D Ultra (version: 13.0.2.3021). Dihedral angles for all relevant groups were set to values between the global minimum and the next local maximum on the conformational energy diagram as calculated by ChemBio3D. These structures were then sequentially refined with B3LYP optimizations using first the 3-21G basis set, followed by the 6-31G(d,p) basis set and finally the 6-311+G(d,p) basis set. The default convergence criteria were used for these preliminary ground state optimizations and for the TD-DFT geometry optimizations of the  $S_1$  and  $T_1$  excited states of **PB1**.

**Ethyl 4-(4-[bis(4-(hexyloxy)phenyl)amino]phenyl)-6-formylthieno[3,4-*b*]thiophene-2-carboxylate (5, DP1-CHO):** Compound **4** (103 mg, 0.26 mmol), 4-(hexyloxy)-*N*-[4-(hexyloxy)phenyl]-*N*-[4-(4,4,5,5-tetramethyl-1,3,2-dioxaborolan-2-yl)phenyl]aniline (TPA-Bpin) (160 mg, 0.28 mmol),  $K_3PO_4$  (165 mg, 0.78 mmol), toluene (6 mL), and  $H_2O$  (0.23 mL), were added to a round-bottomed flask, and the mixture was degassed with  $N_2$  for 20 min.  $[Pd_2(dba)_3]$  (10 mg, 0.011 mmol) and X-phos (20 mg, 0.042 mmol) were then added simultaneously to the reaction mixture. The temperature was then increased to 80 °C and the mixture was allowed to stir for 6 h. The reaction was then diluted with ethyl acetate (200 mL) and extracted using water. The organic layer was separated and dried using  $MgSO_4$ . The solvent was removed under reduced pressure. The product was purified through silica gel chromatography with 10% ethyl acetate/hexanes (0.10 g, 93%).  $^1H$  NMR (500 MHz,  $CDCl_3$ ):  $\delta$  = 9.83 (s, 1H), 7.98 (s, 1H), 7.53 (d,  $J$  = 8.6 Hz, 2H), 7.10 (d,  $J$  = 8.8 Hz, 4H), 6.93 (d,  $J$  = 8.7 Hz, 2H), 6.87 (d,  $J$  = 8.8 Hz, 4H), 4.38 (q,  $J$  = 7.2 Hz, 2H), 3.94 (t,  $J$  = 6.6 Hz, 4H), 1.78 (t,  $J$  = 7.1 Hz, 4H), 1.46 (m, 4H), 1.39 (t,  $J$  = 7.1 Hz, 3H), 1.34 (m, 8H), 0.90 ppm (m, 6H);  $^{13}C$  NMR (125 MHz,  $CDCl_3$ ):  $\delta$  = 178.8, 162.6, 156.5, 150.7, 148.5, 140.8, 139.2, 128.4, 127.6, 127.5, 123.4, 123.3, 118.9, 118.7, 115.6, 115.5, 68.5, 61.9, 31.6, 29.3, 25.8, 22.6, 14.1 ppm (br); IR (neat):  $\tilde{\nu}$  = 3039.7, 2930.1, 2858.2, 1711.8, 1505.6, 1240.6  $cm^{-1}$ ; MS  $m/z$  calcd for  $C_{40}H_{45}NO_5S_2$  [ $M+H$ ]<sup>+</sup>: 683.3; found: 683.4.

**Ethyl 6-formyl-4-(4-(*p*-tolyl)-1,2,3,3a,4,8b-hexahydrocyclopenta[*b*]indol-7-yl)thieno[3,4-*b*]thiophene-2-carboxylate (DP2-CHO):** Synthesis follows the same conditions as for **5**, using 7-(4,4,5,5-tetramethyl-1,3,2-dioxaborolan-2-yl)-4-(*p*-tolyl)-1,2,3,3a,4,8b-hexahydrocyclopenta[*b*]indole (Ind-Bpin) instead of TPA-Bpin (0.04 g, 50%).  $^1H$  NMR (300 MHz,  $CDCl_3$ ):  $\delta$  = 9.83 (s, 1H), 8.04 (s, 1H), 7.49 (s, 1H), 7.46 (s, 1H), 7.21 (s, 4H), 6.87 (d,  $J$  = 8.4 Hz, 1H), 4.91 (t,  $J$  = 6.4 Hz, 1H), 4.41 (q,  $J$  = 7.1 Hz, 2H), 3.90 (t,  $J$  = 8.6 Hz, 1H), 2.37 (s, 3H), 1.93 (m, 2H), 1.74 (m, 2H), 1.59 (m, 2H), 1.41 ppm (t,  $J$  = 7.1 Hz, 3H);  $^{13}C$  NMR (125 MHz,  $CDCl_3$ ):  $\delta$  = 178.8, 162.9, 150.7, 150.0, 140.4, 139.1, 136.5, 133.4, 130.2, 128.4, 124.3, 123.9, 122.6, 121.5, 107.6, 107.5, 69.9, 62.0, 45.2, 35.6, 33.5, 29.9, 24.5, 14.5 ppm; IR (neat):  $\tilde{\nu}$  = 3025.8, 2952.6, 2927.2, 2859.3, 1706.3, 1635.6, 1600.3  $cm^{-1}$ ; HRMS  $m/z$  calcd for  $C_{28}H_{25}NO_3S_2$  [ $M+Na$ ]<sup>+</sup>: 510.1174; found: 510.1280.

**(*E*)-3-(4-(4-[bis(4-(hexyloxy)phenyl)amino]phenyl)-2-(ethoxycarbonyl)thieno[3,4-*b*]thiophen-6-yl)-2-cyanoacrylic acid (6, DP1):** Compound **5** (45 mg, 0.06 mmol) and chloroform (1 mL) were added to a round-bottom flask. The flask was degassed with  $N_2$  for

30 min. Cyanoacetic acid (15 mg, 0.18 mmol) and piperidine (0.04 mL, 0.42 mmol) were then added to the reaction mixture. The flask was then heated to 90 °C and stirred for 1 h. The reaction mixture was then diluted with dichloromethane and acetic acid was added to the mixture. The mixture was extracted with dichloromethane and water, and dried over  $MgSO_4$ . The product mixture was then purified through a silica gel plug with 100% dichloromethane → 3% methanol/dichloromethane → 10% methanol/2% acetic acid/dichloromethane. The solvent was evaporated under reduced pressure. The dye was then extracted in hexanes and water and dried over  $MgSO_4$  to give the final dye (**DP1**) in the form of a purple solid (0.02 g, 51%).  $^1H$  NMR (500 MHz,  $CDCl_3$ ):  $\delta$  = 8.36 (s, 1H), 7.98 (s, 1H), 7.60 (m, 2H), 7.11 (d,  $J$  = 8.85 Hz, 4H), 6.90 (m, 6H), 4.40 (q,  $J$  = 7.2 Hz, 2H), 3.95 (t,  $J$  = 6.3 Hz, 4H), 1.78 (t,  $J$  = 6.9 Hz, 4H), 1.43 (m, 12H), 0.90 (m, 6H), 0.85 ppm (t,  $J$  = 8.94, 3H); IR (neat):  $\tilde{\nu}$  = 3040.5 (br), 2929.3, 2862.1, 2212.9, 1712.1, 1565.8, 1502.6  $cm^{-1}$ ; HRMS  $m/z$  calcd for  $C_{43}H_{46}N_2O_6S_2$  [ $M$ ]<sup>+</sup>: 750.2797; found: 750.2878; UV/Vis ( $CH_2Cl_2$ ):  $\lambda_{max}$  = 558 nm ( $\epsilon$  = 22 000  $M^{-1}cm^{-1}$ ),  $\lambda_{onset}$  = 650 nm; cyclic voltammetry (0.1 M  $Bu_4NPF_6$  in  $CH_2Cl_2$ , sweep width 1.1 to –2.0 V, 0.1  $Vs^{-1}$  scan rate):  $E_{(S+/S)}$  = 1.09 V (vs. NHE).  $E_{(S+/S^*)}$  = –0.79 V [vs. NHE, calcd from  $E_{(S+/S^*)} = (E_{(S+/S)} - E_g^{opt})$ ].

**(*E*)-2-Cyano-3-[2-(ethoxycarbonyl)-4-(4-(*p*-tolyl)-1,2,3,3a,4,8b-hexahydrocyclopenta[*b*]indol-7-yl)thieno[3,4-*b*]thiophen-6-yl]acrylic acid (DP2):** Synthesis follows same procedure as **DP1**. Final product was a purple solid (8 mg, 35%).  $^1H$  NMR (300 MHz,  $CDCl_3$ ):  $\delta$  = 8.33 (s, 1H), 8.01 (s, 1H), 7.51 (br, 2H), 7.20 (brs, 4H), 6.83 (d,  $J$  = 9.24 Hz, 1H), 4.92 (m, 1H), 4.40 (q,  $J$  = 6.33 Hz, 2H), 3.87 (m, 1H), 2.42 (s, 3H), 1.88 (m, 2H), 1.62 (m, 4H), 1.41 ppm (t,  $J$  = 7.1 Hz, 3H); IR (neat):  $\tilde{\nu}$  = 3478.5, 2920.6, 2850.9, 2063.3, 1638.2  $cm^{-1}$ . HRMS  $m/z$  calcd for  $C_{31}H_{26}N_2O_4S_2$  [ $M$ ]<sup>+</sup>: 555.14; found: 555.14; UV/Vis ( $CHCl_3$ ):  $\lambda_{max}$  = 591 nm ( $\epsilon$  = 20 000  $M^{-1}cm^{-1}$ ),  $\lambda_{onset}$  = 670 nm; cyclic voltammetry (0.1 M  $Bu_4NPF_6$  in  $CH_2Cl_2$ , sweep width 1.1 to –2.0 V, 0.1  $Vs^{-1}$  scan rate):  $E_{(S+/S)}$  = 1.08 V (vs. NHE).  $E_{(S+/S^*)}$  = –0.77 V [vs. NHE, calcd from  $E_{(S+/S^*)} = (E_{(S+/S)} - E_g^{opt})$ ].

## Acknowledgements

P.B. and F.G. contributed equally to this work. The authors J.H.D., P.B., G.A.P., and G.S.T. thank the Mississippi NSF-EPSCOR program (EPS-0903787) and the University of Mississippi for funding. J.H.D., P.B., and G.A.P. thank the NSF-CAREER program (NSF-1455167) for support. G.A.P. thanks the UM Sally McDonnell Barksdale Honors College for funding. G.S.T. thanks the NSF MRI award (CHE-1338056) for funding and the Mississippi Center for Supercomputing Research. We also thank Brandon Stamper and Chesney Petkovsek for preliminary X-ray crystallographic analysis. M.K.N., M.G., and F.G. thank the European Community's Seventh Framework Programme (FP7/2007–2013) ENERGY.2012.10.2.1, NANOMATCELL, Grant agreement no: 308997.

**Keywords:** dye-sensitized solar cells · NICS · proaromaticity · solvatochromism · thienothiophene

[1] B. O'Regan, M. Grätzel, *Nature* **1991**, 353, 737.

[2] A. Hagfeldt, G. Boschloo, L. C. Sun, L. Kloo, H. Pettersson, *Chem. Rev.* **2010**, 110, 6595.

[3] M. Grätzel, *J. Photochem. Photobiol. C.* **2003**, 4, 145.

- [4] C. Chen, M. Wang, J. Li, N. Pootrakulchote, L. Alibabaei, C. Ngoc-le, J. Decoppet, J. Tsai, C. Grätzel, C. Wu, S. Zakeeruddin, M. Grätzel, *ACS Nano* **2009**, *3*, 3103.
- [5] M. Sánchez Carballo, M. Urbani, A. K. Chandiran, D. González-Rodríguez, P. Vázquez, M. Grätzel, M. K. Nazeeruddin, T. Torres, *Dalton Trans.* **2014**, *43*, 15085.
- [6] Y. Chiba, A. Islam, Y. Watanabe, R. Komiya, N. Koide, L. Y. Han, *Jpn. J. Appl. Phys. Part 2* **2006**, *45*, L638.
- [7] a) K. Kakiage, Y. Aoyama, T. Yano, T. Otsuka, T. Kyomen, M. Unno, M. Hanaya, *Chem. Commun.* **2014**, *50*, 6379; b) Z. Yao, M. Zhang, H. Wu, L. Yang, R. Li, P. Wang, *J. Am. Chem. Soc.* **2015**, *137*, 3799.
- [8] S. Mathew, A. Yella, P. Gao, R. Humphry-Baker, B. Curchod, N. Ashari-Astani, I. Tavernelli, U. Rothlisberger, M. K. Nazeeruddin, *Nat. Chem.* **2014**, *6*, 242.
- [9] a) B. E. Hardin, H. J. Snaith, M. D. McGehee, *Nat. Photonics* **2012**, *6*, 162; b) J.-H. Yum, T. W. Holcombe, Y. Kim, K. Rakstys, T. Moehl, J. Teuscher, J. H. Delcamp, M. K. Nazeeruddin, M. Grätzel, *Sci. Rep.* **2013**, *3*, 2446; c) J. H. Delcamp, A. Yella, T. W. Holcombe, M. K. Nazeeruddin, M. Grätzel, *Angew. Chem. Int. Ed.* **2013**, *52*, 376; *Angew. Chem.* **2013**, *125*, 394; d) J. H. Delcamp, Y. Shi, J.-H. Yum, T. Sajoto, E. Dell'Orto, S. Barlow, M. K. Nazeeruddin, S. R. Marder, M. Grätzel, *Chem. Eur. J.* **2013**, *19*, 1819; e) A. Dualeh, J. H. Delcamp, M. K. Nazeeruddin, M. Grätzel, *Adv. Energy Mater.* **2013**, *3*, 496; f) A. Dualeh, J. H. Delcamp, M. K. Nazeeruddin, M. Grätzel, *Appl. Phys. Lett.* **2012**, *100*, 173512.
- [10] W. Liu, I. Wu, C. Lai, C. Lai, P. Chou, Y. Li, C. Chen, Y. Hsu, Y. Chi, *Chem. Commun.* **2008**, 5152.
- [11] S. Franco, J. Garin, N. Baroja, R. Pérez-Tejada, J. Orduna, Y. Yu, M. Lira-Cantú, *Org. Lett.* **2012**, *14*, 752.
- [12] Y. Chen, H. Chou, M. Tsai, S. Chen, J. Lin, C. Yao, K. Chen, *Chem. Eur. J.* **2012**, *18*, 5430.
- [13] A. J. Huckaba, F. Giordano, L. E. McNamara, K. M. Dreux, N. I. Hammer, G. S. Tschumper, S. M. Zakeeruddin, M. Grätzel, M. K. Nazeeruddin, J. H. Delcamp, *Adv. Energy Mater.* **2014**, *5*, 1401629.
- [14] B. Myung-Jin, S.-H. Lee, K. Zong, Y.-S. Lee, *Synth. Met.* **2010**, *160*, 1197.
- [15] W.-H. Chang, L. Meng, L. Dou, J. You, C.-C. Chen, Y. Yang, E. P. Young, G. Li, Y. Yang, *Macromolecules* **2015**, *48*, 562.
- [16] S. Wakim, S. Alem, Z. Li, Y. Zhang, S.-C. Tse, J. Lu, J. Ding, Y. Tao, *J. Mater. Chem.* **2011**, *21*, 10920.
- [17] W. Li, Y. Wu, Q. Zhang, H. Tian, W. Zhu, *ACS Appl. Mater. Interfaces* **2012**, *4*, 1822.
- [18] N. G. Connolly, W. E. Geiger, *Chem. Rev.* **1996**, *96*, 877.
- [19] Q.-T. Yu, J.-Y. Liao, S.-M. Zhou, Y. Shen, J.-M. Liu, D.-B. Kuang, C.-Y. Su, *J. Phys. Chem. C* **2011**, *115*, 22002.
- [20] P. v. R. Schleyer, C. Maerker, A. Dransfeld, H. Jiao, N. J. R. v. E. Hommes, *J. Am. Chem. Soc.* **1996**, *118*, 6317.
- [21] a) G. V. Baryshnikov, R. R. Valiev, N. N. Karaush, B. F. Minaev, *Phys. Chem. Chem. Phys.* **2014**, *16*, 15367; b) G. Sánchez-Sanz, I. Alkorta, C. Trujillo, J. Elguero, *Tetrahedron* **2012**, *68*, 6548; c) Z. Chen, C. S. Wannere, C. Corminboeuf, R. Puchta, P. v. R. Schleyer, *Chem. Rev.* **2005**, *105*, 3842; d) "Ground and Excited State Aromaticity: Design Tools for  $\pi$ -Conjugated Functional Molecules and Materials": C. Dahlstrand, Ph.D. Dissertation, Uppsala University, Uppsala, Sweden, June 5, **2012**.
- [22] H. Fallah-Bagher-Shaidaei, C. S. Wannere, C. Corminboeuf, R. Puchta, P. v. R. Schleyer, *Org. Lett.* **2006**, *8*, 863.
- [23] R. Papadakis, H. Ottosson, *Chem. Soc. Rev.* **2015**, *44*, 6472.
- [24] P. B. Karadakov, *J. Phys. Chem. A* **2008**, *112*, 7303.
- [25] S. Ito, H. Miura, S. Uchida, M. Takata, K. Sumioka, P. Liska, P. Comte, P. Péchy, M. Grätzel, *Chem. Commun.* **2008**, 5194.
- [26] J. Yang, P. Ganesan, J. Teuscher, T. Moehl, Y. Kim, C. Yi, P. Comte, K. Pei, T. W. Holcombe, M. K. Nazeeruddin, J. Hua, S. M. Zakeeruddin, H. Tian, M. Grätzel, *J. Am. Chem. Soc.* **2014**, *136*, 5722.
- [27] A. D. Becke, *J. Chem. Phys.* **1993**, *98*, 5648.
- [28] C. Lee, W. Yang, R. G. Parr, *Phys. Rev. B* **1988**, *37*, 785.
- [29] Gaussian 09, Revision D.01, M. J. Frisch, G. W. Trucks, H. B. Schlegel, G. E. Scuseria, M. A. Robb, J. R. Cheeseman, G. Scalmani, V. Barone, B. Menucci, G. A. Petersson, H. Nakatsuji, M. Caricato, X. Li, H. P. Hratchian, A. F. Izmaylov, J. Bloino, G. Zheng, J. L. Sonnenberg, M. Hada, M. Ehara, K. Toyota, R. Fukuda, J. Hasegawa, M. Ishida, T. Nakajima, Y. Honda, O. Kitao, H. Nakai, T. Vreven, J. A. Montgomery, Jr., J. E. Peralta, F. Ogliaro, M. Bearpark, J. J. Heyd, E. Brothers, K. N. Kudin, V. N. Staroverov, R. Kobayashi, J. Normand, K. Raghavachari, A. Rendell, J. C. Burant, S. S. Iyengar, J. Tomasi, M. Cossi, N. Rega, J. M. Millam, M. Klene, J. E. Knox, J. B. Cross, V. Bakken, C. Adamo, J. Jaramillo, R. Gomperts, R. E. Stratmann, O. Yazyev, A. J. Austin, R. Cammi, C. Pomelli, J. W. Ochterski, R. L. Martin, K. Morokuma, V. G. Zakrzewski, G. A. Voth, P. Salvador, J. J. Dannenberg, S. Dapprich, A. D. Daniels, Ö. Farkas, J. B. Foresman, J. V. Ortiz, J. Cioslowski, D. J. Fox, Gaussian, Inc. Wallingford CT, **2009**.
- [30] F. London, *J. Phys. Radium* **1937**, *8*, 397.
- [31] K. Wolinski, J. F. Hilton, P. Pulay, *J. Am. Chem. Soc.* **1990**, *112*, 8251.

Received: August 12, 2015

Published online on December 2, 2015